A theoretical study of a radiofrequency wave propagation through a realistic turbulent marine atmospheric boundary layer based on large eddy simulation

Victor Darchy, Rémi Douvenot, Stéphane Jamme, Hélène Galiègue

▶ **To cite this version:**

Victor Darchy, Rémi Douvenot, Stéphane Jamme, Hélène Galiègue. A theoretical study of a radiofrequency wave propagation through a realistic turbulent marine atmospheric boundary layer based on large eddy simulation. Waves in Random and Complex Media, 2024, pp.1-24. 10.1080/17455030.2024.2398677 . hal-04677486

HAL Id: hal-04677486
https://hal.science/hal-04677486

Submitted on 26 Aug 2024

HAL is a multi-disciplinary open access archive for the deposit and dissemination of scientific research documents, whether they are published or not. The documents may come from teaching and research institutions in France or abroad, or from public or private research centers.

L'archive ouverte pluridisciplinaire **HAL**, est destinée au dépôt et à la diffusion de documents scientifiques de niveau recherche, publiés ou non, émanant des établissements d'enseignement et de recherche français ou étrangers, des laboratoires publics ou privés.

A theoretical study of a radiofrequency wave propagation through a realistic turbulent marine atmospheric boundary layer based on large eddy simulation

Victor Darchy[a,b], Rémi Douvenot[a], Stéphane Jamme[b] and Hélène Galiègue[a]

[a]ENAC, Toulouse University; [b]ISAE-Supaero, Toulouse University

ARTICLE HISTORY
Compiled August 26, 2024

ABSTRACT
This study aims at modeling and investigating the impact of realistic turbulence inhomogeneity on radiowave propagation by utilizing large eddy simulations (LES). An up-to-date version of the X-LES method for generating realistic turbulent phase screens is first introduced. It combines atmospheric simulations with the classical Tatarski statistical modeling. This method naturally incorporates vertical turbulence inhomogeneity into phase screens at scales resolved by LES. It is then extended to sub-grid scales by weighting statistically generated phase variations with the vertical profile of the turbulent structure constant extracted from atmospheric data. This method is applied to replicate turbulence of a classical tropical marine atmospheric boundary layer. The impact of the generated medium on the propagation of a 10 GHz spherical wave emanating from a Gaussian aperture is analyzed through a statistical study of log-amplitude profiles performed for three different source altitudes. Results first show that contrary to a classical homogeneous turbulence modeling, log-amplitude profiles resulting from the propagation into inhomogeneous turbulence exhibit a statistical heterogeneity strongly dependent of source altitude. Furthermore, classical stochastic phase screen generation from a homogeneous Von-Kármán Kolmogorov spectrum seems to give a statistically significant underestimation of the actual impact of turbulence compared to the X-LES method.

KEYWORDS
split-step propagation; inhomogeneous turbulence; log-amplitude fluctuations; large-eddy simulations; marine atmospheric boundary layer

1. Introduction

The marine atmospheric boundary layer (MABL), which encompasses the region near the ocean surface, introduces a complex interplay of atmospheric phenomena [1], along with scattering effects due to the roughness of the sea surface, that can profoundly impact radio frequency (RF) communications and radar systems [2]. This intricate interaction involves both large-scale refraction effects, such as ducting, and small-scale fluctuations of the refractive index. The ducting effect is defined by channels of enhanced refractive index along the sea surface. These ducts can bend or even guide RF signals over considerable distances beyond the normal line-of-sight range. The characterization as well as the modeling of these large-scale atmospheric effects is the

CONTACT V. Darchy. Email: victor.darchy-ext@enac.fr / vdarchy@gmail.com

object of numerous studies [3–5]. Their impact on electromagnetic (EM) wave propagation now can be accurately modeled. However, precise understanding and modeling of small-scale phenomena remain open problems.

Tropospheric turbulence results in a chaotic disturbance of thermodynamic fields, leading to fast variations in the refractive index responsible for scintillation effects. The random and multi-scale behavior of this phenomenon makes its modeling very complex. Nevertheless, in the case of propagation over large distances at frequencies higher than the X-band, these small fluctuations can impair both the phase and the amplitude of the propagating signal [6–8]. A precise modeling of this turbulence is therefore crucial to quantify and anticipate its impact on received signals.

The split-step wavelet (SSW) method is one of the split-step techniques used for simulating long-range propagation in various complex media. This iterative algorithm solves the discrete wide-angle formulation of the parabolic wave equation (PWE) [9,10]. The SSW method follows the same resolution scheme as the classical discrete split-step Fourier method (DSSF) [11]. For every propagation step, the PWE is initially solved in either the spectral domain (for DSSF) or the wavelet domain (for SSW) to account for the propagation in vacuum. Then, to incorporate the influence of the atmosphere, a phase shift is applied. It is modeled through a phase screen, which is theoretically obtained by integrating the refractive index fields on each propagation step. Under the assumption of forward propagation, the PWE also allows for the consideration of the presence of a ground and relief [10,12]. This way, split-step methods enable the handling of numerous propagation scenarios within large environments.

The stochastic multiple phase screen method (sMPS) is widely used to model atmospheric turbulence effects on EM propagation [6,8,13]. It is based on the Tatarski theory [14] which consists in considering the turbulent phase screen as a stochastic process where the phase variations are modeled as random variables. In this approach, the statistical behavior of these phase fluctuations due to turbulence is described by a Kolmogorov spectrum [15]. Although Kolmogorov spectra are commonly used to generate the phase screens, they do not capture all the complexities of real atmospheric turbulence. In actual conditions, turbulence can exhibit different behaviors that show statistical properties depending on various factors such as altitude, weather, and geographical location. Therefore, using a simplified Kolmogorov model does not provide an accurate representation of the turbulence encountered in specific scenarios. In particular, the Kolmogorov theory assumes that turbulence is locally homogeneous and isotropic [15]. In the MABL, strong gradients resulting from heat and moisture exchanges between the atmosphere and the ocean surface induce significant vertical inhomogeneities. Under these conditions, the use of classical Kolmogorov spectra seems at least questionable. Indeed, recent studies have highlighted the non-negligible impact of turbulence inhomogeneities on the propagation of an EM wave [16]. Furthermore, Kolmogorov spectra only describe the statistical behavior of scales within the inertial range of the turbulent flow which can be quite narrow and does not take into account all the scales of eddies into the turbulent flow.

To accurately capture the dynamics of turbulent flows at large scales, previous studies suggest to generate phase screens using large-eddy simulations (LES) of the atmospheric boundary layer [17–19]. This numerical method for solving the Navier-Stokes equations aims at resolving large-scale turbulent structures while modeling the effects of smaller scales [20], known as sub-grid scales (SGS), which are beyond the resolution of the numerical grid. Indeed, the smallest resolved scales are too large to be naturally broken by physical viscous dissipation. Thus, through a sub-grid model, characterized by a SGS diffusion ν_{SGS}, the dissipation is artificially enhanced in the

simulation to prevent energy accumulation at the smallest resolved scales.

However, due to limitations in computational time, the LES grid cannot be as detailed as the propagation grid. Consequently, the smaller sub-grid scales have to be modeled using the Tatarski theory. This approach is referred to as extended-LES method (X-LES) and consists in extending the turbulent behavior observed at resolved scales to sub-grid scales [17].

In this paper, an up-to-date version of X-LES is applied to generate turbulent phase screens representative of a tropical MABL. The objective is to highlight the influence of realistic turbulence on RF beam propagation. Special attention is given to the effect of the vertical inhomogeneity of the turbulent intensity. A local metric of field variation is introduced to quantify its impact. Then, a parametric study on the altitude of the electromagnetic source is performed. The results are compared to those obtained in the case of a homogeneous statistical modeling of turbulence. Doing so, the importance of an accurate modeling of turbulence is highlighted.

This article is organized as follows. Section 2 reminds theoretical aspects of EM wave propagation in turbulent media using phase screens. The updated version of X-LES method used in this study for generating realistic phase screens is then introduced in Section 3 before being applied to the case of a tropical MABL in Section 4. Then, Section 5 presents numerical results aiming at highlighting the influence of inhomogeneous turbulence on RF signal propagation. Finally, Section 6 summarizes our findings and suggests several perspectives for future works.

2. Theory

The aim of this section is to introduce the theoretical context of this study. The iterative SSW solving method for the 2D-PWE used in this paper is first presented and an overview of tropospheric turbulence and its stochastic modeling for EM propagation developed by Tatarski is then proposed. This notably allows to highlight the limitations of certain assumptions in the context of radiofrequency (RF) propagation in a turbulent ABL.

Hereinafter, the propagation is computed in free space in a 2D domain of size $L_x \times L_z$. u indicates the classical reduced scalar electromagnetic field [10] that is here discretized along the vertical axis so that $u(x,z) = u(x, p_z\Delta_z)$ for p_z in $[0, N_z]$, where Δ_z denotes the vertical mesh parameter of the propagation domain.

2.1. Split-step wavelet propagation algorithm

A discretized formulation of the parabolic equation theory is particularly suitable for numerical implementation, aiming at minimizing numerical errors. This approach is commonly referred to as an auto-coherent method [11].

The propagation of an EM wave is described by the well-know Helmholtz equation. In a discretized environment, this can be written as

$$\frac{\partial^2 u}{\partial x^2} - 2jk_0\frac{\partial u}{\partial x} + \mathbf{d}_z^2 u + k_0^2(n^2-1)u = 0, \tag{1}$$

where k_0 indicates the EM wavenumber in vacuum, n is the tropospheric RF refractive index and $\mathbf{d}_z^2$ represents the second-order centered finite-difference operator. Following

a similar reasoning as in the conventional continuous "wide angle" parabolic equation development [10], the discrete forward parabolic wave equation (PWE) is given by [11]

$$\frac{\partial u}{\partial x} = \left[-jk_0(n-1) - j\left(\sqrt{k_0^2 + \mathbf{d}_z^2} - k_0\right)\right] u. \tag{2}$$

In split-step methods, equation (2) is iteratively solved in two steps. The EM field is first propagated in vacuum ($n = 1$) on a propagation step Δ_x. Then, a phase shift defined as $\exp(-j\Phi_{x+\Delta_x})$ is applied to the propagated field to account for the contribution of the atmosphere. $\Phi_{x+\Delta_x}$ stands for the 1D vertical phase screen corresponding to the portion of medium located between x and $x + \Delta_x$ and is theoretically obtained at every z by

$$\Phi_{x+\Delta_x}(z) = k_0 \int_x^{x+\Delta_x} (n(x', z) - 1)\mathrm{d}x'. \tag{3}$$

In this study, numerical simulations of EM propagation are performed using the open-source software "SSW-2D" [21], that is based on the SSW algorithm [9]. This algorithm shares the same formalism as the DSSF algorithm, with a key distinction: the propagation in vacuum is computed in the wavelet domain rather than Fourier and is achieved through a fast wavelet transform (FWT) [22]. Wavelet bases show notable invariance and compression properties that make this decomposition algorithm faster than the fast Fourier transform (FFT), justifying the choice of the SSW method.

Similarly to the DSSF approach, the iterative SSW solution of equation (2) is expressed as

$$u(x + \Delta_x, z) = e^{-j\Phi_{x+\Delta_x}(z)} \mathcal{W}^{-1}[\mathcal{P}\mathcal{W}(u(x, z))]. \tag{4}$$

Here, $\mathcal{W}$ represents the FWT, and $\mathcal{P}$ is the free-space propagator in the wavelet domain. The latter is a dictionary of propagators, computed and stored prior to the initial iteration [12]. Initially, the electric field at position x is decomposed into the chosen wavelet basis, characterized by a decomposition level $L = 3$, using a FWT [22]. It is then represented in the wavelet domain by its corresponding wavelet coefficients. Subsequently, individual wavelets undergo vacuum propagation over a step Δ_x using the dictionary of propagators to obtain new wavelet coefficients. Finally, the field at $x+\Delta_x$ is reconstructed in the spatial domain through an inverse FWT. It then remains to compute $\Phi_{x+\Delta_x}$ and apply the corresponding phase shift to obtain the real electric field at $x + \Delta_x$. The generation of the turbulent phase screens is explained in the following sections.

2.2. Stochastic modeling of tropospheric turbulence

In the lower troposphere, the thermodynamic fields chaotically evolve over time at every point in space, leading to small-scale variations in the refractive index that cause fast fluctuation in the amplitude and phase of the EM signal. Turbulence is a mode of irregular flow that superimposes random agitation on the mean motion of a fluid. Thus, the refractive index is often modeled through a decomposition into a

deterministic mean part and a random fluctuating part such that

$$n = \langle n \rangle + \Delta n, \tag{5}$$

where $\langle n \rangle$ and Δn represent the mean and turbulent components of the refractive index, respectively, and $\langle \cdot \rangle$ denotes spatial averaging. This article only focuses on the specific impact of turbulence on EM wave propagation. In the following, the mean part is therefore supposed homogeneous such that $\langle n \rangle = 1$. The impact of turbulence on an EM signal is thus modeled by a 1D vertical turbulent phase screen given by

$$\Phi_{x+\Delta_x}(z) = k_0 \int_x^{x+\Delta_x} \Delta n(x', z) \mathrm{d}x'. \tag{6}$$

Turbulence, as defined by Richardson [23], is a multi-scale phenomenon. Indeed, multiple turbulent structures of various scales coexist within a turbulent flow. Their behavior is linked to the distribution of initially produced kinetic energy across different flow scales. The classical theory of homogeneous and isotropic turbulence developed by Kolmogorov [15] has identified three main scale ranges, as illustrated in Figure 1. The first zone corresponds to the largest structures responsible for energy production. The scales involved are flow-dependent, as their behavior is conditioned by the geometry of the problem. In the second zone, known as the inertial subrange, turbulent kinetic energy is transferred to smaller scales with a constant decay rate proportional to $k^{-5/3}$, where $k = \frac{2\pi}{l}$ is the spatial wavenumber related to the structure of scale l under consideration. This domain is delimited by two characteristic scales. The outer-scale length L_{os} denotes the largest eddy within the inertial subrange while the inner-scale length L_{is} indicates the smallest one. Finally, in a third zone corresponding to the smallest scales of the flow, nonlinear processes become negligible, and kinetic energy is rapidly dissipated by viscous forces.

The universal behavior of scales within the inertial subrange is well suited to a statistical description of the turbulent phenomenon. The stochastic multiple phase screen method (sMPS) [6,8,24] arises from Tatarski's theory [14] and models the turbulent phase screen as a stochastic process such that $\Phi \sim \mathcal{N}(0, S_\Phi)$ where $\mathcal{N}$ denotes a normal distribution and S_Φ is a Kolmogorov-type scintillation spectrum. In this paper, the classical Von-Kármán Kolmogorov spectrum [25], adapted to fit the discretized auto-coherent theory [24], is employed and is given by

$$S_\Phi(k_z) = 2\pi k_0^2 \Delta_x 0.055 C_n^2 \left(k_z^2 + \left(\frac{2\pi}{L_{\mathrm{os}}} \right)^2 \right)^{-4/3}. \tag{7}$$

In the above equation C_n^2 represents the turbulent structure constant, which characterizes the amplitude of fluctuations in the turbulent refractive index, while k_z denotes the vertical component of the spectral variable.

Although widely used, this stochastic generation method using the Von-Kármán Kolmogorov spectrum relies on strong assumptions and thus has obvious limitations. Firstly, the saturation effect imposed by the Von-Kármán Kolmogorov spectrum in the production zone does not accurately represent the actual energetic behavior of the largest scales of the turbulent flow. Additionally, studies have highlighted the impact of the vertical inhomogeneity of turbulence on the propagation of an EM wave [16–18].

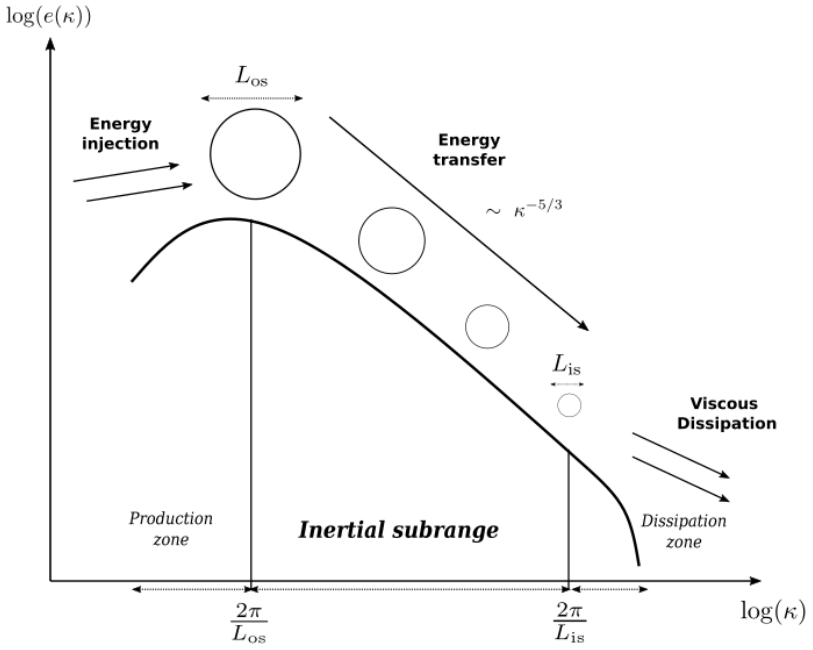

Figure 1. Schematic representation of the turbulent kinetic energy (TKE) spectrum and the different subrange of scales.

In the context of ABL propagation, where strong vertical inhomogeneities occur [26], homogeneous modeling of turbulence may appear too simplistic.

In the next section, we present a method for generating realistic phase screens based on LES results of a MABL. This is widely inspired by the X-LES developed by Gilbert *et al.* [17] but it differs in the algorithm employed to extract the vertical profile of the refractive index structure constant. This profile is subsequently used to introduce vertical inhomogeneity in the modeling of turbulence at sub-grid scales. This approach enables to overcome the two main limitations of the sMPS method. Firstly, LES accurately captures the behavior of large scales in turbulent flows. Additionally, this method allows for the generation of realistic turbulence that is representative of the dynamics of an ABL. In particular, our study highlights the impact of turbulence inhomogeneity in a MABL on RF propagation.

3. Realistic phase screen generation method

The LES is used to numerically solve the filtered versions of the governing equations to yield three-dimensional (3D) turbulent fields representing the largest and most energetic scales within a turbulent flow. In the practical case of generating an ABL, LES allows for the computation of 3D instantaneous fields of thermodynamic variables within an atmospheric domain of size $l_x \times l_y \times l_z$ down to a grid resolution $d_x \times d_y \times d_z$ which precision is constrained by obvious computational capabilities. In particular, for RF applications, these current limitations prevent the generation of full-scale atmospheric domains ($\sim$km) at resolutions that align with the mesh requirements for RF wave propagation ($\sim$cm). To overcome this issue, Gilbert *et al.* [17] proposed to extend LES fields to finer resolution using stochastic generation. This so-called X-LES

method consists in considering every field f as the combination of two contributions such that

$$f(x, y, z, t) = f^{\mathrm{r}}(x, y, z, t) + f^{\mathrm{s}}(x, y, z, t), \tag{8}$$

where f^{r} represents the component of the field associated with scales directly resolved by LES, and f^{s} is a stochastic field that models the contribution of sub-grid scales.

The objective of this section is to precisely develop the formalism of the X-LES method that is used in this paper to generate realistic turbulent phase screens from atmospheric simulation. As in equation (8), the 1D turbulent vertical phase screen is here modeled by a resolved phase Φ^{r} and a sub-grid phase Φ^{s} as

$$\Phi = \Phi^{\mathrm{r}} + \Phi^{\mathrm{s}}. \tag{9}$$

Particular attention is given to the sub-grid phase generation with a focus on the evaluation method of the refractive index structure constant that differs from that used in [17].

3.1. Resolved scales

The resolved phase Φ^{r} is directly derived from LES outputs. The tropospheric RF refractive index is expressed as

$$n = 1 + N \times 10^{-6}, \tag{10}$$

with N the refractivity given by [27]

$$N = 77.60\frac{p}{T} - 9.00\frac{pq_{\mathrm{t}}}{T} + 6.035 \times 10^{5}\frac{pq_{\mathrm{t}}}{T^2}, \tag{11}$$

where p, T, and q_{t} denote the instantaneous atmospheric pressure, absolute temperature, and specific humidity, respectively. At every instant, the resolved scales refractive index field n^{r} is first computed at every LES grid point $(x, y, z) = (i_x d_x, i_y d_y, i_z d_z)$ with $(i_x, i_y, i_z) \in [1, n_x] \times [1, n_y] \times [1, n_z]$ from thermodynamic outputs using equations (10) and (11). The turbulent component Δn^{r} is subsequently derived by subtracting the mean value obtained on the horizontal plane such that

$$\Delta n^{\mathrm{r}}(x, y, z, t) = n^{\mathrm{r}}(x, y, z, t) - \langle n^{\mathrm{r}}(x, y, z, t)\rangle_{(x,y)}\,, \tag{12}$$

where $\langle\cdot\rangle_{(x,y)}$ indicates the mean operator over a – statistically homogeneous – horizontal plane. In the following, the time dependence is omitted. Additionaly, we remind that the objective is here to compute 1D turbulent phase screens to perform 2D propagation. The y-dependency is thus supressed and phase screens computations are performed at an arbitrary chosen y-location. The turbulent phase screen associated with the contribution of resolved scales Φ^{r} over a propagation step is finally computed as

$$\Phi^{\mathrm{r}}_{x+\Delta_x}(z) = k_0 \int_{x}^{x+\Delta_x} \Delta n^{\mathrm{r}}(x', z)\mathrm{d}x'. \tag{13}$$

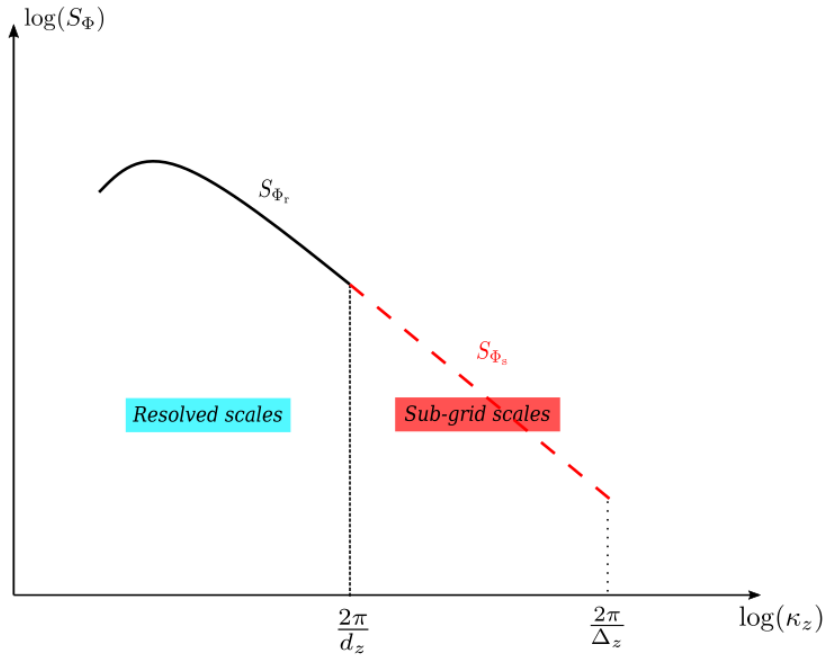

Figure 2. X-LES vertical phase spectrum representation.

Note that the propagation step must satisfy $\Delta_x > d_x$. Interpolation enables obtaining a vertical phase profile with the same numerical precision $\Delta_z < d_z$ as the chosen propagation grid vertical spacing. Nevertheless, at this step of the process, the energetic contribution of the sub-grid scales of the turbulent flow is missing, necessitating the extension of resolved phase variations to finer scales.

3.2. Sub-grid extension

This extension process has been introduced by Gilbert *et al.* [17] and is reminded here. This consists in an hybridization between LES and the Tatarski theory. Indeed, under the assumption that the LES mesh parameter $d = \sqrt[3]{d_x d_y d_z}$ lies in the inertial subrange of scales of the turbulent flow, the resolved phase spectrum can be extended with a Kolmogorov spectrum to account for the energetic contribution of sub-grid scales down to the resolution required for propagation. A schematic representation of the X-LES method is given in Figure 2 from a spectral point of view.

In practice, the sub-grid component of the inhomogeneous phase screen Φ^{s} is generated following [16,17]

$$\Phi^{\mathrm{s}}(z) = \sqrt{C_n^2(z)}\tilde{\Phi}^{\mathrm{s}}(z). \tag{14}$$

$C_n^2(z)$ denotes the vertical profile of the structure constant computed from LES data that is representative of the generated medium. Its evaluation method is detailed further in this section. $\tilde{\Phi}^{\mathrm{s}}$ is a C_n^2-normalized and statistically homogeneous phase screen. This is a purely theoretical phase realization generated from an artificial Kolmogorov

spectrum $S_{\tilde{\Phi}^{\mathrm{s}}}(k_z)$ derived from equation (7) with C_n^2 set to 1:

$$S_{\tilde{\Phi}^{\mathrm{s}}}(k_z) = \begin{cases} 2\pi k_0^2 \Delta_x 0.055 \tilde{C}_n^2 k_z^{-8/3}, & \text{if } k_z \in \left[\frac{2\pi}{d_z}, \frac{2\pi}{\Delta_z}\right], \\ 0 & \text{otherwise.} \end{cases} \tag{15}$$

Note that the term in L_{os} does not appear here as only a part of the inertial regime of turbulence is generated. The use of equation (14) amounts to introducing *a posteriori* a realistic vertical inhomogeneity of the turbulence intensity in the sub-grid phase screen. At each altitude, the variations of the generated phase are weighted by the local value of C_n^2. Note that this development is similar to the one carried out in [17], with the noticeable difference that the inhomogeneous extension operation is here directly performed in 1D on the phase rather than on the 2D refractive index.

3.3. Evaluation of the refractive index structure constant

In our study, the structure constant of the refractive index is directly evaluated from LES outputs following the algorithm proposed by Wilson and Fedorovich [28]. This relies on the Obukhov law [29,30] stating that the statistical fluctuation of the refractive index is steady over the inertial subrange of scales. This is written as

$$C_n^2(z) = \frac{D_n(r,z)}{r^{2/3}}, \ \forall\ r \in [L_{\mathrm{is}}, L_{\mathrm{os}}]\,. \tag{16}$$

In the above equation, r indicates the separation distance and D_n is the autocorrelation function of the refractive index. For radiofrequency wavelengths, the impact of dissipative scales of turbulence on the propagation signal is negligible [6]. Moreover, in the lower troposphere, the inner-scale length is at most of the order of centimeters. Since the LES mesh resolution cannot achieve such precision, the condition $r > L_{\mathrm{is}}$ is always satisfied. Therefore, the direct application of equation (16) only requires knowledge of L_{os} at each altitude. It is to be noted that the evaluation of the outer scale parameter remains a very open problem. As emphasized by Klipp [31], even its physical representation varies depending on the application context. It is here defined as the largest scale above which the power spectral density of the turbulent flow no longer follows a $-5/3$ slope.

The direct computation of L_{os} from LES outputs is, therefore, not straightforward. However, its value in the x-direction is usually linked to the corresponding integral length scale L_x, with $L_{\mathrm{os}|x} \approx \frac{1}{6} L_x$ according to [32]. This formula is empirical and may not be optimal. However, this is not critical since the outer scale length is only used here to set the validity framework for equation (16). Specifically, L_{os} does not play a role in generating turbulent sub-grid phase screens from equation (15). By substituting the expression for L_x, $L_{\mathrm{os}|x}$ follows

$$L_{\mathrm{os}|x}(z) = \frac{1}{6} \int_0^\infty D_{q_{\mathrm{t}}}(r_x, z) \mathrm{d}r_x, \tag{17}$$

where r_x is the separation distance in the x-direction and $D_{q_{\mathrm{t}}}$ represents the autocorrelation function of specific humidity given by

$$D_{q_{\mathrm{t}}}(r_x, z) = \left\langle \left[q_{\mathrm{t}}(x + r_x, z) - q_{\mathrm{t}}(x, z) \right]^2 \right\rangle. \tag{18}$$

Note that $D_{q_t}(r_x, z)$ here indicates the autocorrelation between two specific humidity vectors of size n_y located at (x, z) and $(x + r_x, z)$, respectively. The $L_{\mathrm{os}|x}$ value is computed at each time step and for each altitude to obtain a vertical profile averaged over time. For the sake of simplicity, and since this article focuses on the homogeneity hypothesis, we assume an isotropic modeling of turbulent structures in our study giving $L_{\mathrm{os}} = L_{\mathrm{os}|x}$.

Algorithm 1 details the numerical evaluation of the structure constant of the refractive index in the x-direction for given altitude and time. This is approximately the same algorithm as the one proposed in [28]. In particular, since C_n^2 is a critical parameter of the X-LES method, the autocorrelation function of the refractive index is calculated pointwise, unlike the algorithm for computing L_{os}. The difference with [28] lies in the limiting criterion imposed on r_x concerning the validity of equation (16). In [28], the maximum value of r_x is constant with z and is graphically derived from the plot of the autocorrelation function of the refractive index at a given altitude of interest. In the present case, the maximum value of r_x varies with z regarding the vertical profile of the calculated $L_{\mathrm{os}}(z)$. As for the the outer scale parameter, the isotropy assumption is applied to the structure constant of the refractive index and leads to $C_n^2|_x = C_n^2|_y = C_n^2|_z = C_n^2$. This hypothesis is quite common and usually satisfied in the case of convective boundary layers [18,28].

The generation of turbulent phase screens using the X-LES method thus occurs in two steps. The contribution of scales directly resolved by LES is simply obtained through the integration of the refractive index fluctuations over a propagation step. The observed phase variations are extended to sub-grid scales from a Kolmogorov spectrum, following the same principle as the sMPS method. This phase extension is representative of the generated medium since the sub-grid phase screen is *a posteriori* multiplied by the time-averaged $\sqrt{C_n^2(z)}$ computed from LES outputs. This process allows for the consideration of the inhomogeneity of turbulence that is characteristic of an ABL at every scale. In the next section, this method is applied to the case of a tropical MABL.

Algorithm 1 Computation of $C_n^2|_x(z,t)$

Require: instantaneous resolved scales turbulent refractive index $\Delta n^{\mathrm{r}}(x,y,z,t)$, LES domain size l_x and l_y, LES discretization step d_x, $L_{\mathrm{os}}(z)$
Ensure: $C_n^2|_x(z,t)$ instantaneous structure function parameter at altitude z
  for $i_x \in [1, L_{\mathrm{os}}(z)//d_x]$ **do**
    $r_x \leftarrow i_x \times d_x$ set separation distance
    $i_{\mathrm{s}} \leftarrow 0$ initialize the counter
    $s \leftarrow 0$ initialize temporary sum
    for $y \in [0, l_y]$ **do**
      for $x \in [0, l_x]$ **do**
        if $x + r_x \leq l_x$ **then**
          $s \leftarrow s + [\Delta n^{\mathrm{r}}(x + r_x, y, z, t) - \Delta n^{\mathrm{r}}(x, y, z, t)]^2$ evaluation of local structure function
          $i_{\mathrm{s}} \leftarrow i_{\mathrm{s}} + 1$
        end if
      end for
    end for
    $D_{\Delta n}(r_x, z) \leftarrow s/i_{\mathrm{s}}$ mean structure function at z for separation distance r_x
    $C_n^2|_x(r_x, z, t) \leftarrow D_{\Delta n}(r_x, z)/r_x^{2/3}$ value of C_n^2 at z for separation distance r_x
  end for
  $C_n^2|_x(z,t) \leftarrow \frac{L_{\mathrm{os}}(z)}{d_x} \sum_{r_x = d_x}^{L_{\mathrm{os}}(z)} C_n^2|_x(r_x, z, t)$ mean over the different r_x

4. Generation of a turbulent marine atmospheric boundary layer for long range propagation

In this study, atmospheric simulations are to be regarded as a tool for investigating the impact of realistic inhomogeneous turbulence, representative of a turbulent ABL, on RF propagation. In particular, this study does not aim at undertaking an in-depth investigation of the generation of a turbulent ABL through LES.

In this section, the X-LES method is applied to generate turbulent phase screens from a well documented LES case of a Barbados Oceanographic and Meteorological EXperiment (BOMEX) shallow cumulus MABL [18,33,34]. This scenario results in a non-precipitating shallow cumulus layer located between 500 m and 1500 m in altitude above the ocean. Given that specific humidity is the primary factor influencing RF tropospheric scintillation, this moist MABL case is well-suited for our study.

4.1. Large eddy simulation of a marine atmospheric boundary layer

Simulations are perfomed with the open-source computational fluid dynamics code MicroHH [34] developped for LES in the atmosphere and in which Siebesma's BOMEX case is implemented [33,34]. The complete model setup can be found in [33].

In this study, we use an atmospheric domain of size $l_x \times l_y \times l_z = 5 \times 5 \times 3$ km. Periodic boundary conditions are applied in both x and y directions while a free-slip boundary condition is set at the top the domain and surface fluxes are governed by the Monin-Obukhov similarity theory [30]. Note that MicroHH uses the Smagorinsky-Lilly SGS-model [35]. The simulated medium is resolved down to a grid resolution of $d_x \times d_y \times d_z =$

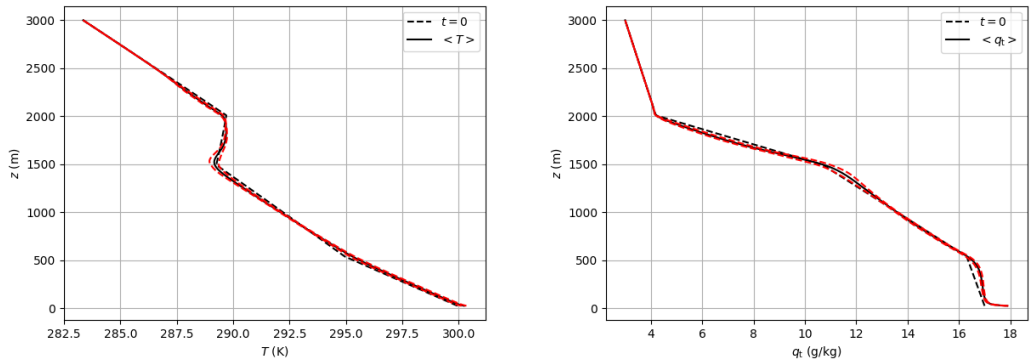

(a) Absolute temperature.

(b) Specific humidity.

Figure 3. Absolute temperature (a) and specific humidity (b) mean vertical profiles averaged over the last 3 hours (black plain line) along with the corresponding initial profiles (black dashed line). Red dashed lines indicate the temporal variability of these mean profiles.

$5\times5\times5$ m. Such mesh precision is more than sufficient to achieve solution convergence. It notably exceeds that employed in similar RF propagation studies [17,18] but aligns with the empirical recommendations outlined in [36] concerning LES of convective boundary layers. This is, to the author's knowledge, the finest LES grid resolution ever used for the study of RF propagation in an ABL. The interest here in choosing the finest possible resolution is to ensure that the majority of the turbulent energy contained in the X-LES phase screens is generated with near-exact accuracy from atmospheric simulations, ensuring the highest possible precision in our turbulence modeling.

The evolution of the generated medium is computed over a period of 6 hours, with the initial 3 hours dedicated to the convergence of the simulation towards a statistically steady solution. During the last 3 hours of the simulation, instantaneous 3D thermodynamic fields are recorded every $\tau = 10$ min. Simulations are run on 500 processors using high performance computing (HPC) ressources.

Figure 3 shows the absolute temperature and the specific humidity vertical profiles averaged over the last 3 hours of the simulation on the horizontal plane. The red dashed lines delimit the interval of twice the standard deviation of the successively saved domains. The negligible variability with time of these mean thermodynamic profiles indicates that the simulation effectively converges towards a statistically steady mean solution. Furthermore, it is important to note the temperature gradient inversion between 1500 and 2000 m. This inversion is indicative of a stable vertical stratification, which is characteristic of the entrainment zone of a convective atmospheric boundary layer.

4.2. Phase screens computation

Vertical profiles of the structure constant of the refractive index and the outer scale parameter are necessary for the use of the X-LES method to generate the sub-grid component Φ^{s} of the phase screens in equation (9). The mean profiles of L_{os} and C_n^2 averaged over the last 3 hours of simulated time in our computation domain are plotted in Figure 4(a) and 4(b), respectively. As expected, the outer scale length globally grows

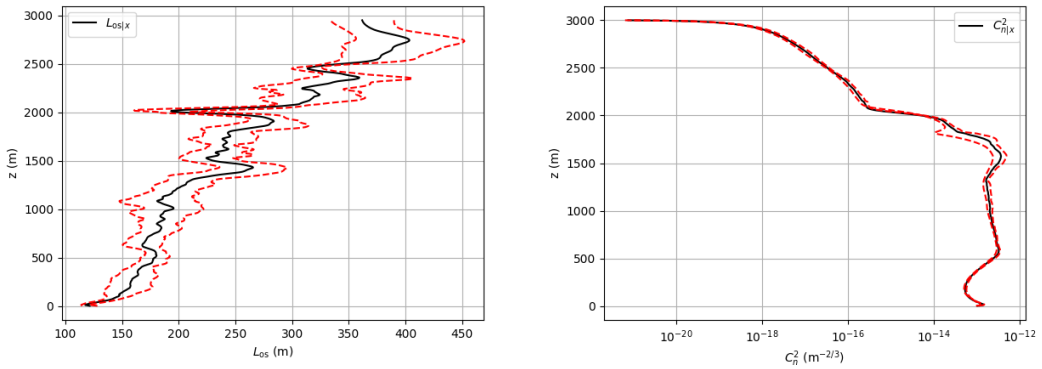

(a) $L_{\mathrm{os}}(z)$. (b) $C_n^2(z)$.

Figure 4. Outer scale length (a) and structure constant of the refractive index (b) mean vertical profiles averaged over the last 3 hours of the computations. Red dashed lines indicate the temporal variability of these mean profiles.

with altitude, in particular above $z = 2000$ m in the free atmosphere. This vertical profile is used to compute the structure parameter of the refractive index at each altitude using algorithm 1. The variation of C_n^2 with altitude plotted in Figure 4(b) highlights a significant vertical inhomogeneity in the turbulence intensity across the studied domain. Indeed, it clearly shows two different regimes of turbulence. Strong turbulence is located below 2000 m, more specifically between 500 m and 1600 m within the generated shallow cumulus layer, while it is clearly negligible above 2000 m in the free atmosphere. Thus, no impact on the propagated signal is *a priori* expected for radio frequencies at these altitudes. This profile is directly used in equation (14) to generate inhomogeneous phase screens at sub-grid scales Φ^{s}.

Figure 5 shows a 2D $\Delta n(x, z)$ map at arbitrary chosen instant and y-position. It is directly obtained from LES outputs using equations (11) and (12). The observed behavior is identical to that identified in the C_n^2 profile with significant variations in the refractive index within the convective cloud layer. We also notice a quite evident difference in organization of turbulence between the entrainment layer, located between 1500 m and 2000 m in altitude, and the mixing layer below. While the fluctuations in refractive index exhibit a chaotic dynamics below 1500 m, we observe a periodic vertical stratification of these variations between 1500 m and 2000 m. As mentioned in Section 4.1, the temperature gradient inversion observed between 1500 m and 2000 m in Figure 3(a) indicates a stable stratification characteristic of the entrainment zone of a convective atmospheric boundary layer. In a stratified entrainment layer, the stable atmosphere inhibits convection and promotes the propagation of internal gravity waves [37]. These gravity waves induce periodic vertical movements of air particles, thereby creating a more organized vertical structure in the turbulent fluctuations of the refractive index. Indeed, gravity acts as a restoring force that tends to restore the vertical equilibrium of the atmosphere, thereby favoring the coherent vertical propagation of turbulent perturbations. The internal gravity waves generated in this layer thus lead to periodic upward and downward oscillations of air particles, resulting in a appearance of periodic vertical structure in the refractive index fluctuations.

On the contrary, in the convective mixing layer, turbulence is dominated by buoyancy-driven thermal phenomena associated with shear, which prevents the oc-

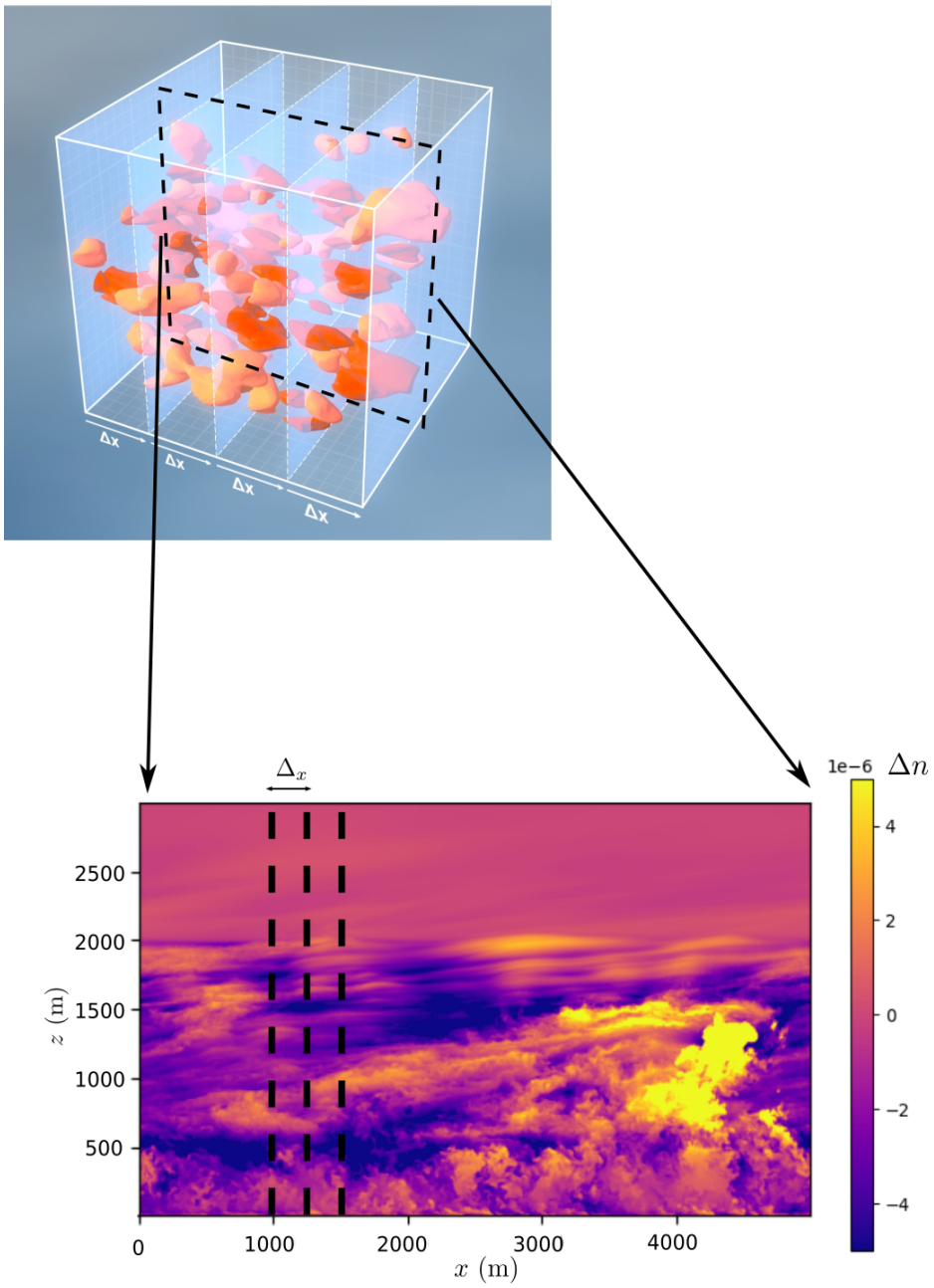

Figure 5. Extraction of a 2D mapping of turbulent refractive index fluctuations at a specific time and arbitrary chosen y-position within the simulated LES domain using MicroHH. Dashed lines indicate the integration step of Δn used to compute phase screens at resolved scales Φ^{r}. Note that the 3D domain is a schematic representation of one LES domain.

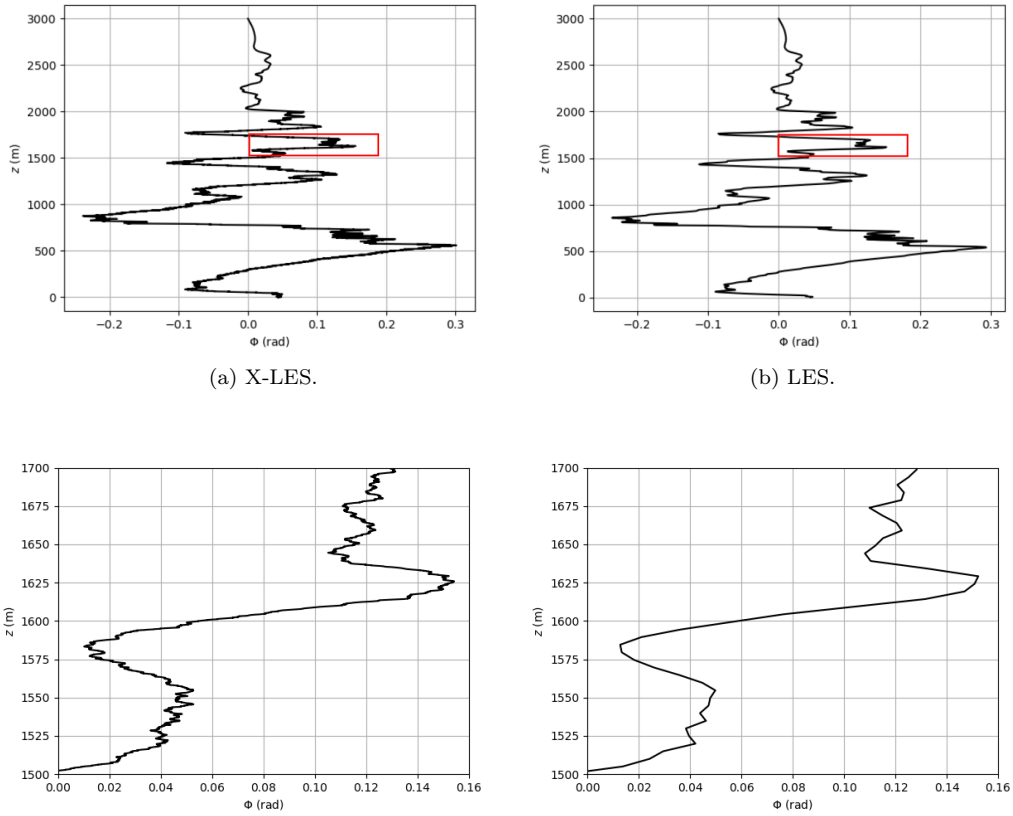

(a) X-LES. (b) LES.

(c) X-LES (zoom). (d) LES (zoom).

Figure 6. Examples of phase screens generated with (a) the X-LES method, (b) directly resolved LES fields. (c) and (d) are zoomed views of (a) and (b) in the area between 1500 m and 1700 m delineated by a red rectangle in these figures.

currence of gravity waves and leads to a chaotic distribution of refractive index fluctuations as depicted in the 2D instantaneous $\Delta n(x, z)$ map in Figure 5 below 1500 m.

The resolved scales phase screens Φ^{r} are computed by integrating these refractive index fluctuations on the considered propagation step Δ_x that is here set to 250 m. This process is repeated on the entire length of the LES domain which leads to the computation of 20 turbulent phase screens over a 5 km range. The full scale turbulent phase screens Φ are ultimately obtained by combining Φ^{r} and Φ^{s}.

Figure 6(a) presents an example of a phase screen generated using the X-LES method, while Figure 6(b) shows the same screen without the extension of phase variations, only using equation (13) with a propagation step $\Delta_x = 250$ m and an EM wavenumber k_0 corresponding to a frequency of 10 GHz. As mentioned in Section 4.1 the atmospheric simulation is here highly resolved. Therefore, the contribution of subgrid scales Φ_{s} is barely noticeable in Figure 6(a). Figures 6(c) and 6(d) are zoomed views of the altitude range from 1500 m to 1700 m, providing a clearer distinction of the small phase variations induced by the X-LES method. Similarly, the impact of phase fluctuations at unresolved scales Φ^{s} on the propagation results is also minimal in our case. This is explained by the fact that the turbulent energy generated with the sMPS method at scales smaller than 5 m – that corresponds to the LES grid pa-

rameter – has a small impact on the propagation of a 10 GHz radiowave. However, it should be noted that conducting atmospheric simulations at such fine grid resolutions is extremely costly. The methodological interest of X-LES primarily lies in the rapid generation of sub-grid scale phase screens through a stochastic approach and it is, of course, more viable to work at coarser LES grid resolutions for which a preliminary study on this issue [38] has shown that the impact of the extension process would be more significant.

The generated vertical phase screens are inhomogeneous in the z direction and it appears that the amplitude of the phase fluctuations statistically follow the same vertical evolution as the C_n^2 profile with the most significant phase variations located below 2000 m. Furthermore, it is worth noting that the vertical inhomogeneity is also conveyed by the sub-grid phase. In particular, almost no sub-grid variations Φ_s are added to the phase profile above 2000 m.

4.3. Extension to long range propagation

The effect of turbulence accumulates as the signal propagates through the medium. In the context of RF systems, its impact becomes noticeable after several tens of kilometers. However, as specified in Section 3, it is currently impractical to generate turbulent domains of such dimensions at the necessary resolution. This issue was addressed in [17] using the ergodicity principle. Indeed, since a periodic boundary condition is applied in the propagation direction, it is possible to juxtapose LES domains saved at uncorrelated instances to artificially extend the propagation domain. The physical decorrelation time is simply defined as the ratio $\tau = l_x / < U >$, where $< U >$ is the mean flow velocity in the propagation direction averaged over the last 3 hours of the simulation. In the present case, it is equal to 10 minutes. Thus, for each instantaneous set of data, phase screens are computed using the previously presented X-LES method and stored. During the propagation process, screens are randomly selected to mitigate the occurrence of correlation phenomena on the observed results.

Figure 7 displays the average turbulent phase profile calculated from the 380 screens generated from the concatenation of 19 atmospheric domains. It is first remarkable that the calculated mean profile is clearly not centered, contrary to the modeling assumption classicaly made with the sMPS method – which involves generating turbulent phase from Gaussian white noise. Furthermore, the plot of the standard deviation interval (red dashed lines) once again highlights that the variability of the profile is governed by the vertical profil of the refractive index structure constant C_n^2.

In the following, we propose to study the free-space propagation of a spherical EM wave at a frequency of 10 GHz for a source located at different altitudes corresponding to various turbulent intensity zones. This aims at highlighting the impact of inhomogeneous turbulence on the propagated signal.

5. Numerical simulations

The impact of turbulence on the amplitude of an EM signal is often quantified by the evolution with range of the log-amplitude variance [6,8,14], denoted as σ_χ^2 and given

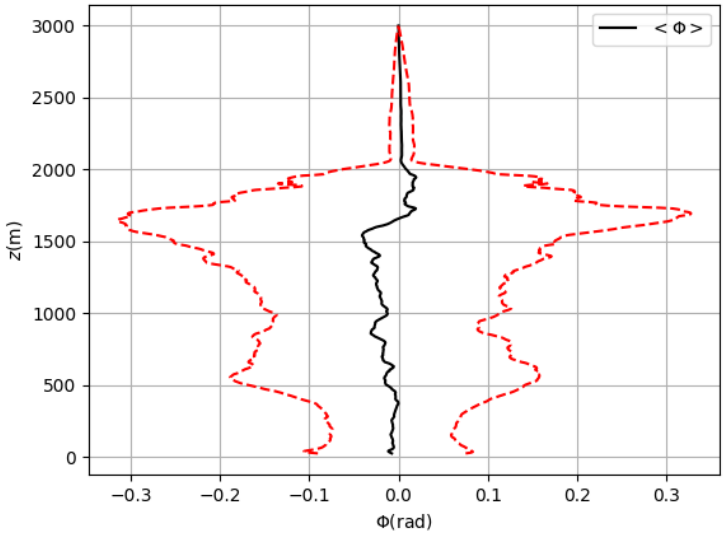

Figure 7. Average phase screen calculated from the 380 samples obtained from the simulation of 19 atmospheric domains via MicroHH (solid black line). The dashed red lines indicate the interval plus or minus the standard deviation.

by $\langle \chi^2 \rangle_z - \langle \chi \rangle_z^2$, where the log-amplitude χ is defined as

$$\chi(z) = \ln\left(\frac{|\mathbf{E}_\mathrm{t}(z)|}{|\mathbf{E}_0(z)|}\right). \tag{19}$$

In the above equation, $\mathbf{E}_\mathrm{t}$ indicates the propagated electric field in the considered turbulent medium while $\mathbf{E}_0$ is the field that would have been obtained at the same point in an atmosphere without turbulence. The variance along the vertical axis of the log-amplitude σ_χ^2 illustrates the specific effect of atmospheric perturbations on the amplitude of the electric field by quantifying its intensity variations around a certain mean.

This metric has two important limitations for our study. Firstly, σ_χ^2 only provides a global quantitative measure of the turbulence effect, losing any information about localization. While this information may be of little importance in the case of a classical modeling with a homogeneous Kolmogorov spectrum, it is in our case crucial to assess the influence of turbulence inhomogeneity on EM propagation. Secondly, as illustrated in Figure 4(b), the generated turbulence is here strongly inhomogeneous over the 3000 m vertical window. It is quite strong between 0 m and 1800 m and weak, even negligible, above 2000 m. It is therefore legitimate to consider that studying the variability of the propagation signal around an arithmetic mean calculated over the entire vertical range is not an appropriate approach in this study.

Thus, we introduce the log-amplitude vertical profile $\chi(z)$ at different ranges in order to retain local information regarding the impact of inhomogeneous turbulence and to provide a comprehensive qualitative interpretation of the phenomenon. The obtained profiles result from averaging over $N_\mathrm{simu} = 500$ simulations to give a local statistical estimation of the turbulence influence on propagation.

In this theoretical investigation, the free-space propagation of a 10 GHz frequency

spherical wave emanating from a complex source point (CSP) [39] representing a Gaussian aperture with a width of 6λ, located at $x_s = 50$ m before the first turbulent phase screen and at different altitudes z_s, is studied over a range of 95 km. This distance corresponds to the concatenation of 19 atmospheric domains saved at 10-minutes intervals during the last 3 hours of the simulation. The propagation step Δ_x is set to 250 m while the vertical parameter of the propagation grid Δ_z is equal to $5/3\lambda = 0.05$ m. Simulations are performed with the open-source SSW-2D software [21].

In order to highlight the influence of vertical turbulence inhomogeneity on the propagation of a spherical RF signal, simulations are conducted for three different source altitudes. The two first altitudes are respectively of 600 m and 1600 m, corresponding to the two local peaks of turbulence intensity observed on the vertical profile of C_n^2 in Figure 4(b). A third altitude of 2250 m is studied where turbulence is negligible.

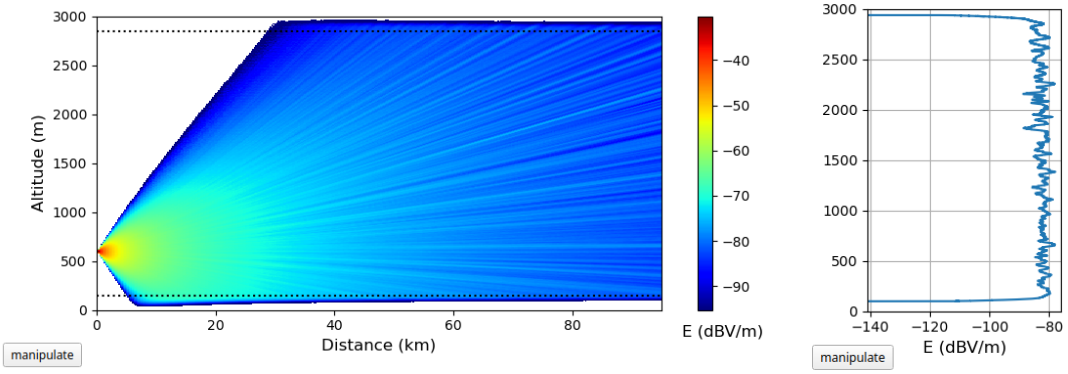

(a) Total E-field. (b) Final E-Field.

Figure 8. (a) Complete propagation of an electric field from a CSP located at an altitude of 600 m simulated with SSW 2D. (b) Vertical profile of the final electric field from the same scenario.

Figure 8(a) depicts one sample of the evolution of the complete electric field amplitude as a function of distance for $z_s = 600$ m, in which the effect of turbulence is noticeable through the appearance of interference patterns. Horizontal dashed lines located at 150 m and 2850 m indicate absorbing conditions applied to the propagation signal to prevent from numerical reflections [10]. Figure 8(b) shows the vertical profile of the final field amplitude obtained once the signal has crossed the whole horizontal domain. As highlighted above, it is not possible to draw conclusions about the effect of an inhomogeneous turbulence model compared to the classical homogeneous model based on this result alone. Indeed, the random nature of turbulence necessitates a statistical study for a relevant comparative analysis.

The mean log-amplitude profiles computed at $x = 60$ km and $x = 95$ km are plotted in colored solid lines for three different source altitudes in Figure 9. These three configurations for which phase screens are generated with the X-LES method are compared to an equivalent homogeneous turbulence case plotted in black line. For this reference simulation, the classical sMPS is used to randomly generate phase screens every Δ_x from a Von-Kármán Kolmogorov spectrum introduced in equation (7). In this formula, both the structure constant of the refractive index and the outer scale length are set to the mean value of the profiles obtained from LES results in Section 4 that are plotted in Figure 4, giving $C_n^2 = 1.23 \times 10^{-13}$ m$^{-2/3}$ and $L_{os} = 246$ m.

Figure 9 first demonstrates that unlike what is obtained with a classical homogeneous modeling, log-amplitude vertical profiles resulting from the propagation of a

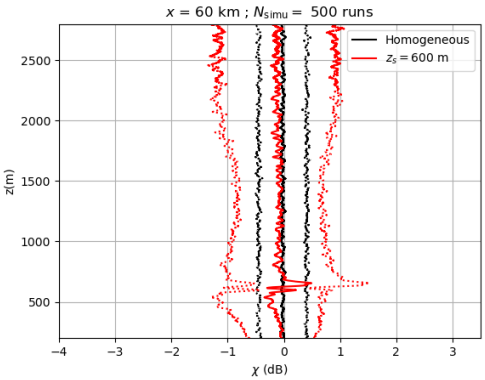

(a) $z_s = 600$ m ; $x = 60$ km.

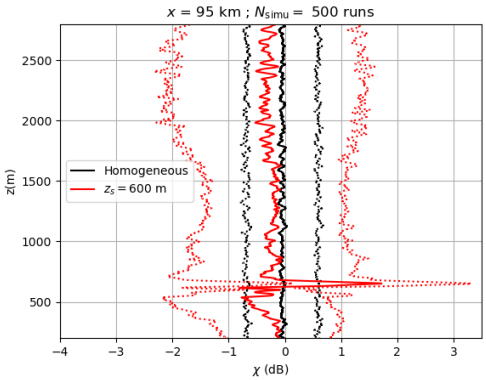

(b) $z_s = 600$ m ; $x = 95$ km.

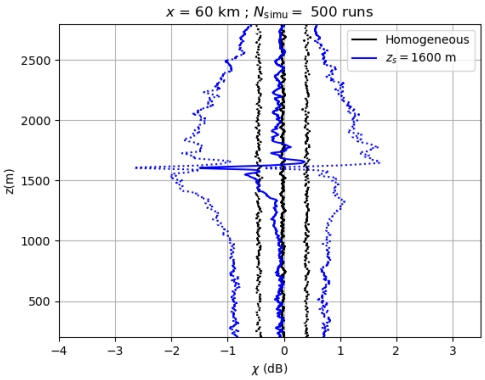

(c) $z_s = 1600$ m ; $x = 60$ km.

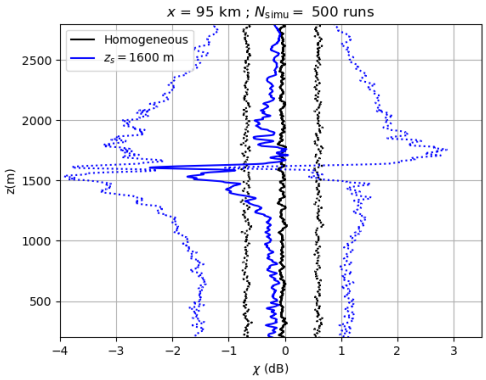

(d) $z_s = 1600$ m ; $x = 95$ km.

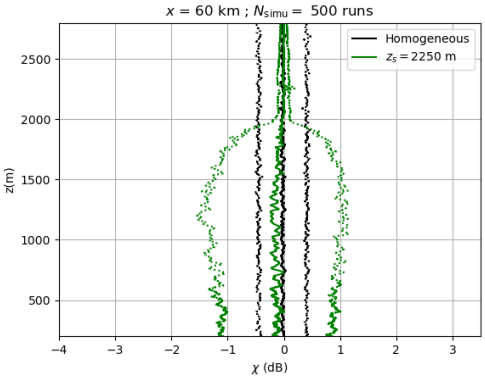

(e) $z_s = 2250$ m ; $x = 60$ km.

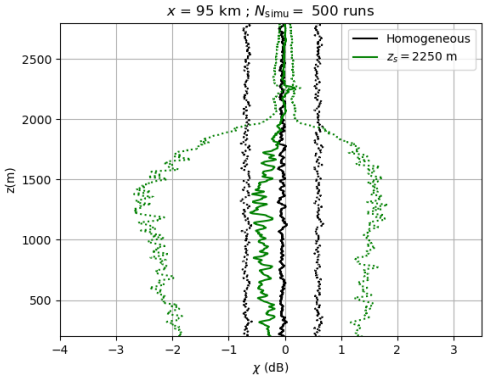

(f) $z_s = 2250$ m ; $x = 95$ km.

Figure 9. Comparison of vertical profiles of log-amplitude averaged over 500 simulations at 60 km (a)(c)(e) and 95 km (b)(d)(f) ranges resulting from X-LES propagation of an electric field generated by a complex point source located at z_s of 600 m (red), 1600 m (blue), and 2250 m (green). The black curve corresponds to the profile obtained for propagation through screens generated from an equivalent homogeneous Von-Kármán Kolmogorov spectrum. Dashed lines indicate the range of variation within plus or minus one standard deviation.

spherical wave within realistic turbulence are statistically inhomogeneous. Note that for a homogeneous statistical modeling, the effect of turbulence on signal propagation

is independent of the source altitude. Indeed, in this configuration, since the generated turbulence is statistically homogeneous in x and z, its effect on the spherical wavefront is independent of both the propagation angle and the source altitude. It also indicates that, in this case, phase screens generation from a homogeneous Von-Kármán Kolmogorov spectrum leads to a statistically possible underestimation of the effects of turbulence on the propagation signal.

A complementary study to this paper was conducted in [40], addressing an inhomogeneous and purely stochastic modeling of turbulence. The results obtained show that while accounting for the vertical inhomogeneity of turbulence also leads to a statistical heterogeneity of the log-amplitude profile compared to the equivalent homogeneous modeling, the local discrepancies observed are less significant than those obtained here. Thus, this overall underestimation by the classical sMPS method is both due to the stochastic Gaussian generation method and to the failure to account for the vertical inhomogeneity of the medium.

Furthermore, χ profiles resulting from propagation in inhomogeneous turbulence depend on z_s. Indeed, when the source is located in a region of high turbulence, a variation peak is observed in the log-amplitude profile in the area around z_s. The comparison between plots at 60 and 95 km ranges also illustrates that this behavior is cumulative with range: the observed peak intensifies as the EM wave progresses. The occurrence of this fluctuation peak can be explained by the accumulation of strong variations of the refractive index in the main direction of propagation. Indeed, since the source under study is spherical, the rays propagate in different directions. In particular, the more grazing the propagation angle, the more turbulence the ray traverses along its path. Therefore, if the source is placed in a region of strong turbulence, a significant and statistically quasi-homogeneous phase shift accumulates on the wavefront in this region during propagation. The high amplitude of the fluctuation peak observed in Figures 9(a)(b)(c)(d) is explained by the fact that at altitudes of 1600 m and 600 m, the phase fluctuations encountered are not zero-mean, as indicated by Figure 7, contrary to the classical modeling of the sMPS method, which assumes that the turbulent phase screens are centered Gaussian processes. Thus, the observed cumulative effect is even more significant.

On the contrary, the green curve corresponding to the case for which the source is positioned at 2250 m, in a region where turbulence is negligible, shows the absence of such a peak. Ultimately, the value of χ at a given position, as well as its variability characterized by the interval of plus or minus the standard deviation (dashed lines), are strongly dependent on the turbulence encountered along the propagation path.

Therefore, considering the differences between the log-amplitude profile that results from a homogeneous stochastic modeling and that obtained from the realistic approach using the X-LES method, an accurate modeling of turbulence, in particular its vertical inhomogeneity, is recommended at least in the region between the source and receiver altitudes.

6. Discussion and conclusion

The objective of this study was to model and study the impact of turbulence inhomogeneity on radiowave propagation. In this article, a revised version of the X-LES method [17] for generating realistic inhomogeneous turbulent phase screens has first been presented. It consists in an hybridization between atmospheric simulations and the classical statistical modeling of turbulence [14]. In this method, the vertical inho-

mogeneity of turbulence is naturally carried by the phase screens for scales directly resolved with LES. It has been here *a posteriori* extended to the sub-grid scales by directly weighting phase variations that are randomly generated following the sMPS method by the $\sqrt{C_n^2(z)}$ profile extracted from the atmospheric simulations. The algorithm used to calculate the vertical profile of the refractive index structure constant differs from that in [17] and is inspired by the one proposed in [28], which involves utilizing the Obukhov relation at each altitude. We also proposed to vary the validity domain of this formula with altitude by calculating the value of the outer scale length L_{os} at each z of the LES domain.

This method has been applied to generate realistic phase screens representative of a BOMEX tropical MABL [33], for which the turbulence intensity is vertically inhomogeneous. The effect of this turbulent medium on the propagation of an EM wave in the X-band has then been analyzed through a statistical study of the vertical profile of the resulting log-amplitude. This original metric provides a local statistical estimation of the turbulence impact, particularly suitable when studying inhomogeneous turbulence. The resulting vertical profiles of log-amplitude, averaged over 500 simulations and bounded by the interval plus or minus the standard deviation, were examined after 60 and 95 km of propagation for 10 GHz spherical waves originating from Gaussian sources positioned at three different altitudes.

We first pointed out that contrary to that resulting from the equivalent homogeneous sMPS generation method, the log-amplitude profiles obtained in the case of an inhomogeneous modeling of turbulence are statistically heterogeneous. Moreover, the observed log-amplitude profiles were strongly dependent on the source altitude, which can be easily explained. Indeed, considering both a spherical wavefront and a vertically inhomogeneous turbulence, the turbulent intensity encountered by a given ray varies along the propagation path between the source and the considered observation point. We finally noticed that the classical stochastic phase screen generation from a homogeneous Von-Kármán Kolmogorov spectrum statistically underestimates the impact of turbulence on the propagation field compared to X-LES method. It is however important to note that the amplitude of the observed gap is case-dependent and similar studies in different meteorological conditions or using different LES grid resolutions are the subject of future work. To provide more in-depth quantitative results, future work involve accounting for both the uncertainty related to the turbulence statistics themselves and the uncertainty related to the LES simulations of the studied boundary layers.

This gap between the two methods might have two origins. Firstly, the error may arise from the spectrum itself. Indeed, the Von-Kármán Kolmogorov spectrum only provides an approximate estimation, in the form of a saturation effect, of the distribution of refractive index fluctuations related to the turbulence in the production zone. It is to be noted that the latter corresponds to the scales with the highest energy content, as illustrated in Figure 1. Additionally, as indicated in equation (7), the limit of the inertial range and thus the origin of this saturation effect is governed by the value of L_{os}, which is difficult to estimate accurately, as discussed in Section 3.3. Moreover, the use of a Von-Kármán Kolmogorov spectrum assumes that the inertial range is entirely described by a constant ratio in $k_z^{-8/3}$. However, recent studies on non-Kolmogorov turbulence have shown that, actually, this slope varies significantly across different and complex sub-ranges [41]. Finally, the modeling error may also stem from the chosen law to model the phase screen as a stochastic process. In the sMPS method, screens are generated by filtering Gaussian white noise with a Kolmogorov-type spectrum. This approach assumes that phase fluctuations related to turbulence have zero mean. This

assumption seems questionable given the average phase screen profile calculated from atmospheric simulations and plotted in Figure 7. Indeed, it is evident that contrary to the classical modeling, the generated phase screens can't be modeled as centered processes. Moreover, since at a given altitude the phase fluctuation is locally not zero-mean, the resulting localized phase shift statistically accumulates which may be responsible for both the discrepancies between the two methods observed in the estimation of potential losses due to turbulence, and the occurrence of highly localized log-amplitude fluctuation peaks around the source altitude when the latter is located in a region of strong turbulence. It is important to note that the observations made here, particularly regarding the mean phase profile, are highly dependent on the case studied. Studies on other meteorological scenarios are the subject of future work in order to draw conclusions about the assumptions made regarding the origin of the differences between the results obtained with the sMPS and X-LES methods.

In future works, equivalent studies at higher frequencies and on other cases of atmospheric simulations would first be interesting to enrich these initial results. For instance, the study of a stratus layer or precipitating cumulus layer would be of high interest but requires a substantial collaborative work from meteorologists and LES researchers to accurately reproduce such atmospheric boundary layers. Moreover, similar works in complete environments are necessary to quantify the relative effect of turbulence compared to other phenomena such as large-scale refractivity variations or the effects of terrain or sea surface. Thus, a sensitivity analysis would enable to precisely assess the necessity to take turbulence inhomogeneity into account. Also, Finally, it should be noted that in the current version of the X-LES method, phase screens are calculated within atmospheric domains saved at different time instances and then randomly selected to extend the propagation domain while mitigating correlation effects. By doing so, one of the advantages of LES, which allows for generating a medium with controlled physical correlation, is lost. It would therefore be judicious to utilize the periodicity of boundary conditions in the propagation direction as well as the knowledge of the generated medium dynamics to determine the optimal data saving time and thereby proposing a propagation through realistically correlated and ordered phase screens.

Acknowledgements

The authors would like to thank the Centre National d'Études Spatiales (CNES) and the Fédération de recherche ENAC ISAE-SUPAERO ONERA (FONISEN) for the funding as well as Dr. Chiel van Heerwaarden for his support in the use of the MicroHH code. This work was performed using HPC resources from CALMIP (Grant 2023-P22033).

Disclosure statement

No potential conflict of interest was reported by the authors.

References

[1] R. C. Beardsley, C. E. Dorman, C. A. Friehe, L. K. Rosenfeld, and C. D. Winant. Local atmospheric forcing during the coastal ocean dynamics experiment: 1. A description of the marine boundary layer and atmospheric conditions over a northern california upwelling region. *Journal of Geophysical Research: Oceans*, 92(C2):1467–1488, 1987.

[2] D. E. Kerr. *Propagation of Short Radio Waves*, volume 24. IET, 1987.

[3] H.V. Hitney, J.H. Richter, R.A. Pappert, K.D. Anderson, and G.B. Baumgartner. Tropospheric radio propagation assessment. *Proceedings of the IEEE*, 73(2):265–283, 1985.

[4] R. Douvenot, V. Fabbro, P. Gerstoft, C. Bourlier, and J. Saillard. A duct mapping method using least squares support vector machines. *Radio Science*, 43(06):1–12, 2008.

[5] N. E. Lentini and E. E. Hackett. Global sensitivity of parabolic equation radar wave propagation simulation to sea state and atmospheric refractivity structure. *Radio Science*, 50(10):1027–1049, 2015.

[6] V. Fabbro and L. Feral. Comparison of 2D and 3D electromagnetic approaches to predict tropospheric turbulence effects in clear sky conditions. *IEEE Transactions on Antennas and Propagation*, 60(9):4398–4407, 2012.

[7] Y-H. Chou and J-F. Kiang. Ducting and turbulence effects on radio-wave propagation in an atmospheric boundary layer. *Progress In Electromagnetics Research B*, 60:301–315, 2014.

[8] S. Mukherjee and C. Yardim. Accurate computation of scintillation in tropospheric turbulence with parabolic wave equation. *IEEE Transactions on Antennas and Propagation*, 69(8):4748–4757, 2021.

[9] H. Zhou, R. Douvenot, and A. Chabory. Modeling the long-range wave propagation by a split-step wavelet method. *Journal of Computational Physics*, 402:109042, 2020.

[10] D. Dockery and J.R. Kuttler. An improved impedance-boundary algorithm for Fourier split-step solutions of the parabolic wave equation. *IEEE Transactions on Antennas and Propagation*, 44(12):1592–1599, 1996.

[11] H. Zhou, A. Chabory, and R. Douvenot. A 3D split-step Fourier algorithm based on an discrete spectral representation of the propagation equation. *IEEE Transactions on Antennas and Propagation*, 65(1988-1995), 2017.

[12] T. Bonnafont, R. Douvenot, and A. Chabory. A local split-step wavelet method for the long range propagation simulation in 2D. *Radio Science*, 56(2):1–11, 2021.

[13] D. L Knepp. Multiple phase-screen calculation of the temporal behavior of stochastic waves. *Proceedings of the IEEE*, 71(6):722–737, 1983.

[14] V. I. Tatarskii. *The Effects of the Turbulent Atmosphere on Wave Propagation.* Israel Programm for Scientific Translations, 1971.

[15] A. Kolmogorov. The local structure of turbulence in incompressible viscous fluid for very large Reynolds' numbers. *Akademiia Nauk SSSR Doklady*, 30:301–305, 1941.

[16] M. Wagner, P. Gerstoft, and T. Rogers. Estimating refractivity from propagation loss in turbulent media. *Radio Science*, 51(12):1876–1894, 2016.

[17] K. E. Gilbert, X. Di, S. Khanna, M. J. Otte, and J. C. Wyngaard. Electromagnetic wave propagation through simulated atmospheric refractivity fields. *Radio Science*, 34(6):1413–1435, 1999.

[18] A. Dipankar and P. Sagaut. A new phase-screen method for electromagnetic wave propagation in turbulent flows using large-eddy simulation. *Journal of Computational Physics*, 228:7729–7741, 2009.

[19] S. Avramov-Zamurovic, K. P. Judd, S. Matt, R. A. Handler, A. T. Watnik, J. R. Lindle, J. M. Esposito, and W. A. Jarrett. Propagating beams carrying orbital angular momentum through simulated optical turbulence generated by Rayleigh–Bénard natural convection. *Waves in Random and Complex Media*, 0(0):1–21, 2023.

[20] J. Smagorinsky. General circulation experiments with the primitive equations : I. the basic experiment. *Monthly Weather Review*, 91(3):99 – 164, 1963.

[21] R. Douvenot. SSW-2D: Some open-source propagation software introducing split-step

wavelet and wavelet-to-wavelet propagation techniques. In *2023 IEEE-APS Topical Conference on Antennas and Propagation in Wireless Communications (APWC)*, pages 020–024, 2023.

[22] S. Mallat. A theory for multiresolution signal decomposition: the wavelet representation. *IEEE Transactions on Pattern Analysis and Machine Intelligence*, 11(7):674–693, 1989.

[23] L. F. Richardson. Weather prediction by numerical process. *Quarterly Journal of the Royal Meteorological Society*, 48:282–284, 1922.

[24] V. Darchy, R. Douvenot, H. Galiègue, and S. Jamme. Discrete turbulent spectrum modelling for 2D split-step electromagnetic propagation schemes. In *2023 17th European Conference on Antennas and Propagation (EuCAP)*, pages 1–5, 2023.

[25] T. Von Karman. Progress in the statistical theory of turbulence. *Proceedings of the National Academy of Sciences*, 34(11):530–539, 1948.

[26] M. Chamecki and N. L. Dias. The local isotropy hypothesis and the turbulent kinetic energy dissipation rate in the atmospheric surface layer. *Quarterly Journal of the Royal Meteorological Society*, 130(603):2733–2752, 2004.

[27] A. Tunick. Cn2 model to calculate the micrometeorological influences on the refractive index structure parameter. *Environmental Modelling and Software*, 18(2):165–171, 2003.

[28] C. Wilson and E. Fedorovich. Direct evaluation of refractive-index structure functions from large-eddy simulation output for atmospheric convective boundary layers. *Acta Geophysica*, 60:1474–1492, 2012.

[29] A. M. Obukhov. Structure of the temperature field in a turbulent flow. *Izv. Akad. Nauk SSSR, Ser. Geogr. Geofiz*, 13(1):58–69, 1949.

[30] J. C Wyngaard. *Turbulence in the Atmosphere*. Cambridge University Press, 2010.

[31] C. Klipp. Turbulence anisotropy in the near-surface atmosphere and the evaluation of multiple outer length scales. *Boundary-Layer Meteorology*, 151(1):57–77, 2014.

[32] S.B. Pope and P.J. Eccles. *Turbulent Flows*. Cambridge University Press, 2000.

[33] A. P. Siebesma, C. S. Bretherton, A. Brown, A. Chlond, J. Cuxart, P. G. Duynkerke, H. J., M. Khairoutdinov, D. Lewellen, C. Moeng, E. Sanchez, B. Stevens, and D. E. Stevens. A large eddy simulation intercomparison study of shallow cumulus convection. *Journal of the Atmospheric Sciences*, 60(10):1201 – 1219, 2003.

[34] C. C. van Heerwaarden, B. J. H. van Stratum, T. Heus, J. A. Gibbs, E. Fedorovich, and J. P. Mellado. MicroHH 1.0: a computational fluid dynamics code for direct numerical simulation and large-eddy simulation of atmospheric boundary layer flows. *Geoscientific Model Development*, 10(8):3145–3165, 2017.

[35] D. K. Lilly. Models of cloud-topped mixed layers under a strong inversion. *Quarterly Journal of the Royal Meteorological Society*, 94(401):292–309, 1968.

[36] P. P. Sullivan and E. G. Patton. The effect of mesh resolution on convective boundary layer statistics and structures generated by large-eddy simulation. *Journal of the Atmospheric Sciences*, 68(10):2395 – 2415, 2011.

[37] F. Einaudi and J. J. Finnigan. The interaction between an internal gravity wave and the planetary boundary layer. part i: The linear analysis. *Quarterly Journal of the Royal Meteorological Society*, 107(454):793–806, 1981.

[38] V. Darchy, R. Douvenot, S. Jamme, and H. Galiègue. Investigation on vertical resolution of atmospheric simulations for the propagation in realistic turbulent media. In *2023 IEEE-APS Topical Conference on Antennas and Propagation in Wireless Communications (APWC)*, pages 086–089, 2023.

[39] A. L. Cullen and P. K. Yu. Complex source-point theory of the electromagnetic open resonator. *Proceedings of the Royal Society of London. A. Mathematical and Physical Sciences*, 366(1725):155–171, 1979.

[40] V. Darchy, R. Douvenot, S. Jamme, and H. Galiègue. Electromagnetic wave propagation through realistic inhomogeneous turbulence. *URSI Radio Science Letters*, 5, 2024.

[41] K. Kumari and D. A. Donzis. Regimes of optical propagation through turbulence: theory and direct numerical simulations. *Waves in Random and Complex Media*, 0(0):1–35, 2023.